Invited Paper

Carbon-Based Terahertz Devices

Xiaowei He[a], Weilu Gao[a], Qi Zhang[a], Lei Ren[a], Junichiro Kono[a,b,c]

[a]Department of Electrical and Computer Engineering, [b]Department of Physics and Astronomy, and [c]Department of Materials Science and NanoEngineering, Rice University, Houston, Texas, U.S.A.

ABSTRACT

Carbon nanotubes and graphene are promising for diverse terahertz (THz) device applications. Here, we summarize our recent studies on the THz dynamic conductivities and optoelectronic devices of these materials in the THz region. We show that the THz response of single-wall carbon nanotubes (SWCNTs) is dominated by plasmon oscillations along the nanotubes, which lead to extremely anisotropic THz conductivities. By utilizing the strong THz plasmon resonance as well as its pronounced anisotropy in aligned SWCNT films, we built THz polarizers with perfect performance and polarization-sensitive THz detectors that work at room temperature. In addition, we studied the THz conductivities of graphene samples with and without electrical gating. We demonstrated excitation and active control of surface plasmon polaritons in graphene, as well as a graphene THz modulator with a high modulation depth, a high modulation speed, and a designable resonance frequency.

Keywords: Carbon nanotubes, graphene, terahertz, polarizer, detector, modulator

1. INTRODUCTION

Despite many years of world-wide efforts, mature solid-state device technology is still lacking in the terahertz (THz) frequency range, i.e., electronics and photonics do not overlap. Existing device technologies for the generation, manipulation, and detection of THz radiation are still in their infancy.[1] Recently, there has been increasing recognition that low-dimensional carbon materials, carbon naontubes (CNTs) and graphene, in particular, possess novel optoelectronic and electronic properties[2, 3] that are promising for diverse THz device applications, such as THz emitters, detectors, and polarizers.[4]

In this article, we summarize results of a series of our recent experimental studies on THz optical conductivity measurements and optoelectronic device applications of CNTs[5-7] and graphene in the THz region.[8-10] We showed that the broad absorption peak universally observed for single-wall carbon nanotubes (SWCNTs) at ~4 THz is due to the plasmonic resonance along the tube axis in metallic and doped semiconducting carbon nanotubes.[5] The strongly anisotropic nature of plasmon resonance allowed us to build a perfect THz polarizer based on multiple layers of well-aligned CNT thin films.[6] This polarizer has a degree of polarization of 99.9% and an extinction ratio of ~30 dB, outperforming the conventional THz polarizers (wire-grid polarizers). We also developed a CNT-based THz photodetector with a responsivity of ~2.5 V/W and a detectivity of ~5×10^6 cm-Hz$^{1/2}$/W.[7] Not only can the detector work at room temperature, but it also shows a high degree of polarization sensitivity due to the strong alignment of CNTs. In graphene, we showed that its charge carrier density, and thus, its optical conductivity, can be effectively modified though electrical gating.[8] We further demonstrated how we can efficiently excite and actively control the surface plasmon polaritons (SSPs) in graphene, which can become the building block for diverse graphene-plasmonic devices.[9] We built a high-speed, frequency-controllable THz modulator based on single layer graphene (SGL) with a modulation depth as high as 50%, in which the resonance frequency was tailored to be in a wide THz region by the top metallic apertures.[10]

*kono@rice.edu; phone 1 713 348-2209; fax 1 713 348-3091

Automatic Target Recognition XXV, edited by Firooz A. Sadjadi, Abhijit Mahalanobis,
Proc. of SPIE Vol. 9476, 947612 · © 2015 SPIE · CCC code: 0277-786X/15/$18
doi: 10.1117/12.2185159

2. PLASMONIC TERAHERTZ RESPONSE OF CARBON NANOTUBES

Understanding the dynamic behavior of charge carriers in CNTs in response to THz radiation is the first step toward the development of CNT-based THz devices. Theoretical studies predicted the existence of one-dimensional (1D) plasmons that can be excited along the SWCNT axis.[11] Experimentally, a number of THz/far-infrared spectroscopic studies have been performed.[12-16] One common spectral feature that has been observed repeatedly is a broad THz conductivity peak around 4 THz. This feature was interpreted through two possible mechanisms, one being the interband absorption across the curvature-induced narrow band gap in non-armchair metallic nanotubes,[12-14] and the other being plasmon excitation along tube axis.[15-17]

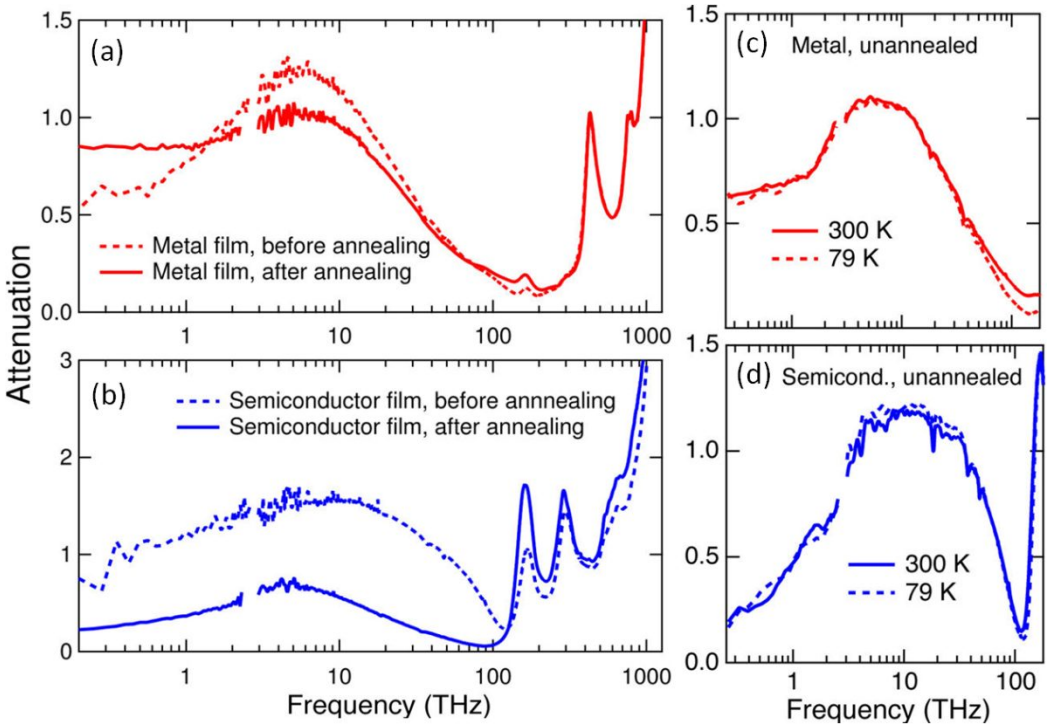

Figure 1. Attenuation spectra of metal- and semiconductor-enriched SWCNT films at room temperature before and after annealing. (a) Metal-enriched SWCNT film before (dashed) and after (solid) annealing. (b) Semiconductor-enriched SWCNT film before (dashed) and after (solid) annealing. Temperature dependence of the THz peak in (c) unannealed metal-enriched film and (d) unannealed semiconductor-enriched film. Adapted from Ref. [5].

To clarify the origin of the peak, we performed absorption spectroscopy studies in a wide spectral range, from the THz to the ultraviolet, on highly metal- and semiconductor-enriched SWCNT films. The broad THz peak was observed in both types of films, but it significantly decreased in semiconductor-enriched films after annealing, which removes dopants, as shown in Figs. 1a and 1b. Moreover, the THz peak of both types of films showed very weak temperature dependence (see Figs. 1c and 1d). If it were due to the curvature effect, the THz peak would be observable only in metallic tubes and strongly temperature dependent. However, both predictions contradict our experimental results. Hence, our results rule out the hypothesis of the curvature effect, providing strong evidence that the THz peak comes from plasma resonance of SWCNTs. Quantitative analysis shows that the complex dynamic conductivity, $\sigma(\omega)$, obtained from transmission spectra can be fit well by a theoretical model including both plasmon resonance and the Drude-like free carrier response,[5] which further confirms the plasmonic nature of the THz peak. As excited in the confined CNT channel, the plasma resonance is strongly polarized, leading to the strongly enhanced anisotropy of THz spectra in aligned CNTs.[18] This pronounced anisotropic property opens up the possibility to build high-performance THz polarizers based on well-aligned CNT films.

3. TERAHERTZ OPTOELERONIC DEVICES BASED ON CARBON NAOTUBES

3.1 Carbon Nanotubes Terahertz Polarizer

Conventional THz polarizers are made by wire-grid metallic wires with uniform spaces, the drawbacks of which are their fragility as well as the finite operation range limited by the structurally tuned architecture.[6] The inherent and strong anisotropic optical properties of CNTs make them ideal candidates for THz polarizer applications with added benefits including mechanical robustness and broadband THz operation. There have been a number of studies on the development of THz polarizers based on aligned CNT films with less ideal performances.[12, 15, 16] Here, we show that a perfect THz polarizer can be made from stacks of extremely aligned SWCNT films (see Fig. 2a).

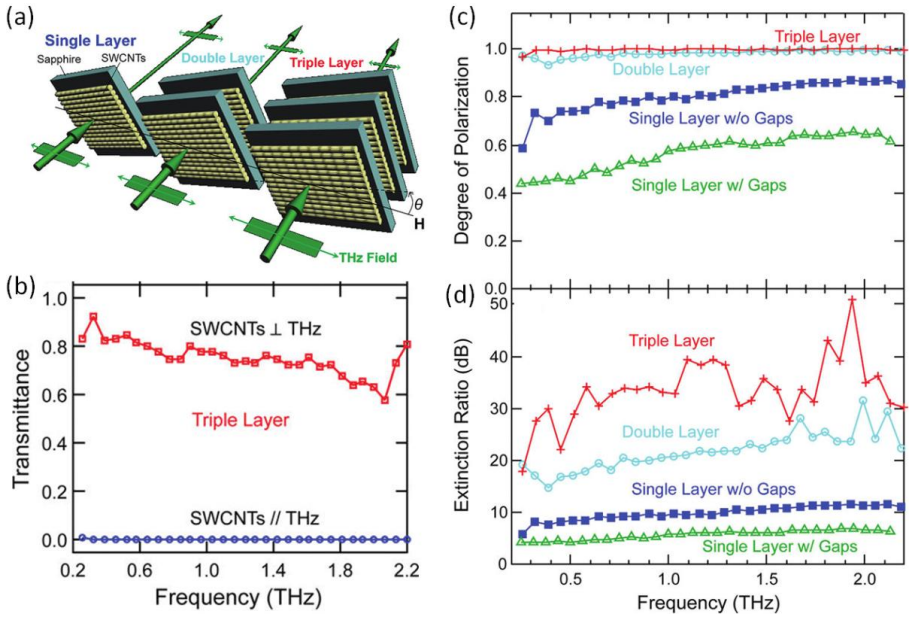

Figure 2. (a) Scheme showing the use of multiple SWCNT films to produce high-performance a THz polarizer. (b) THz transmittance spectra in the 0.2-2.2 THz range for a triple-layer SWCNT film. Blue solid lines with open circle markers are for the parallel case, and red solid lines with open square markers are for the perpendicular case. (c) Degree of polarization and (d) extinction ratio of the THz polarizers with different layer numbers as a function of frequency in the 0.2–2.2 THz range. Adapted from Ref. [6].

Our polarizer is produced through multiple transfers of aligned SWCNT thin films onto a sapphire window. These aligned SWCNT films with a thickness of around 1 μm were grown from photolithography-defined catalysts patterns on silicon substrates by a water-assisted chemical vapor deposition (CVD) method. The THz transmittance spectra of a polarizer made of three layers display extremely strong anisotropy, as shown in Fig. 2b. While it totally blocks THz radiation when the SWCNT alignment direction is parallel to the polarization direction of the incident beam, the polarizer shows very weak interaction with the THz beam in the perpendicular configuration. By carefully comparing the performance of polarizers made by different layers of aligned SWCNTs, one can see that both the degree of polarization (DOP) and extinction ratio (ER) increase with increasing number of SWCNT layers, as shown in Figs. 2c and 2d. For the polarizer with triple layers of SWCNTs, we achieved a 99.9% DOP, an ER of ~30 dB, and broadband performance from ~ 0.4 to 2.2 THz, which outperforms previous CNT-based THz polarizers as well as commercial wire-grid THz polarizers.[6] These experimental results as well as the sample and scalable fabrication method (contact transfer) demonstrate the remarkable utility of aligned SWCNTs for THz technology.

3.2 Carbon Nanotube Terahertz Photodetector

THz detectors are required for a wide range of applications in astronomy, sensing, communications, imaging, and defense. Current THz detectors are mostly cryogenic, narrow-band and bulky.[7] Therefore, entirely novel and new material systems or approaches are being sought. The strong broadband THz absorption from plasmon resonance, the excellent thermal properties, and mechanical strength make CNTs very attractive candidates for

thermal-based THz detection.[19] CNT-based thermal detectors can be divided into two categories: bolometric detectors[20, 21] and photothermoelectric (PTE) detectors.[22, 23] While the former uses a heat-induced conductivity change to detect light, the latter responds to light in the form of a thermal voltage (current) generated through a temperature gradient. The Seebeck coefficient (S) of the detector material is the key factor to affect the performance of a PTE detector. The S of a CNT film is usually less than ~50 μV/K, but it could be largely enhanced through electronic type separation or the incorporation of other polymers;[24, 25] it also can be conveniently turned from p- to n-type by diverse doping methods,[26] allowing for the fabrication of a CNT-PTE detector based on a p-n junction.[7, 22, 23] THz detectors using antennas coupled to CNT quantum dots, individual metallic SWCNTs, and CNT bundles and films have been demonstrated,[27-30] but they work only at low temperatures. Here, we demonstrate a room-temperature-operating, antenna-free, and broadband THz-PTE detector based on aligned SWCNT thin films.[7]

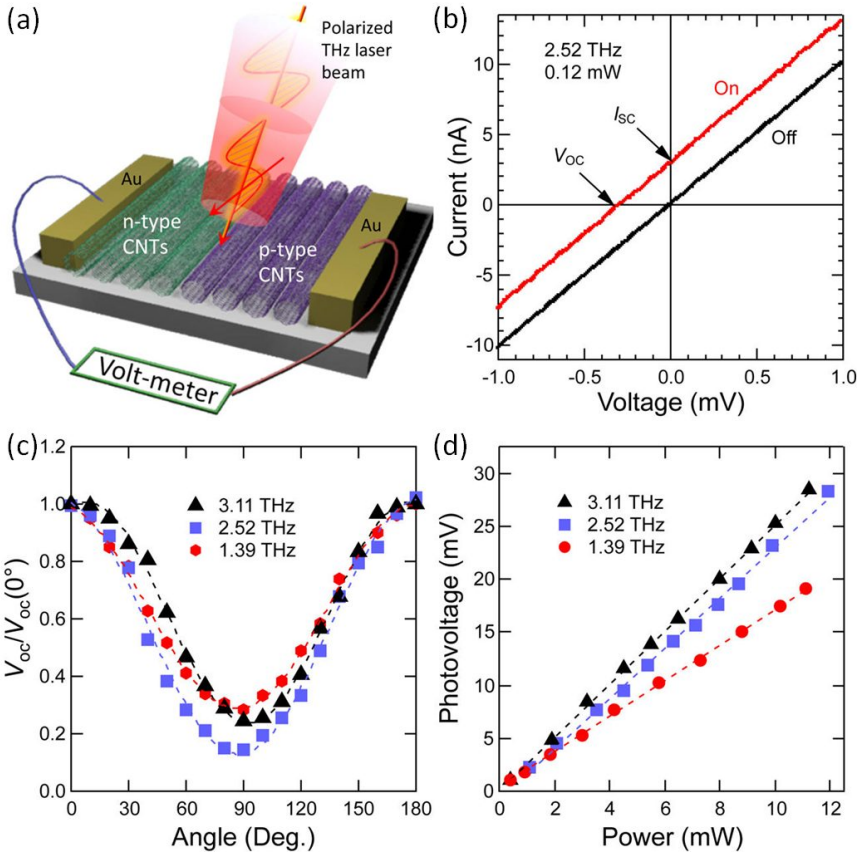

Figure 3. (a) A schematic diagram of the experimental geometry. The I–V characteristics are measured, while the device is illuminated in air at room temperature by a linearly polarized THz beam. (b) Current–voltage characteristic under illumination by a THz beam with a frequency of 2.52 THz (red), and without illumination (black). (c) Polarization dependence of the open-circuit voltage, V_{oc}, normalized by its value for parallel polarization, for frequencies of 1.39 THz, 2.52 THz, and 3.11 THz. (d) Power dependence of V_{oc} for frequencies of 1.39 THz, 2.52 THz, and 3.11 THz, yielding responsivities of 2.5 V/W, 2.4 V/W, and 1.7 V/W, respectively. Adapted from Ref. [7].

This detector was fabricated on a single piece of an aligned SWCNT film grown by the CVD method with thickness around 1-2 μm. The width and length of the detector channel were ~150 μm and ~1 mm, respectively. A p-n junction was made by partially n-doping the as-grown p-type film, as illustrated in Fig. 3a. The whole device was supported on Teflon tape for better thermal isolation from the environment. The open circuit photovoltage, V_{oc}, was observed under THz radiation, giving an average response of ~2.5 V/W, as shown in Figs. 3b and 3d. The NEP of the detector was around 20 nW/ $Hz^{1/2}$, and the estimated detectivity was ~5×10^6 cm-$Hz^{1/2}$/W by considering an active detector area of ~1-mm diameter. The detector essentially works as a thermocouple, in which the difference of S between the n- and p-sides determines its responsivity; the larger the difference, the higher the responsivity.[23] Careful thermal measurements show that in our device the S of the original p-type film is ~70 μV/K, and the S of the

n-type film is ~ −70 μV/K. The large difference of S at the junction is responsible for the observed large photovoltage. The added benefit of the detector is its polarization sensitivity, a unique feature of well-aligned SWCNT films, which could not be realized on the majority of existing thermal detectors. As one can see in Fig. 3c, the ratio of photovoltage between the parallel and perpendicular directions is around 0.1 to 0.3, which is much more pronounced than that in the infrared and visible regions. These results realized uncooled THz detectors based on a macroscopic CNT film. Further improvement in sensitivity can be achieved by: i) increasing the active area by the fabrication of multiple junctions on the same device and ii) using a highly enriched semiconducting SWCNT film to boost the Seebeck coefficients and therefore the responsivity.

4. TERAHERTZ AND INFRARED SPECTROSCOPY OF GATED GRAPHENE

The study of AC dynamics of Dirac fermions in graphene is very important for developing graphene-based THz optoelectronics. While a number of studies have confirmed the so-called universal optical conductivity for interband transitions in a wide spectra range,[31-33] only recently there have been reports about studies of the intraband conductivity in the THz region.[8, 34-36]

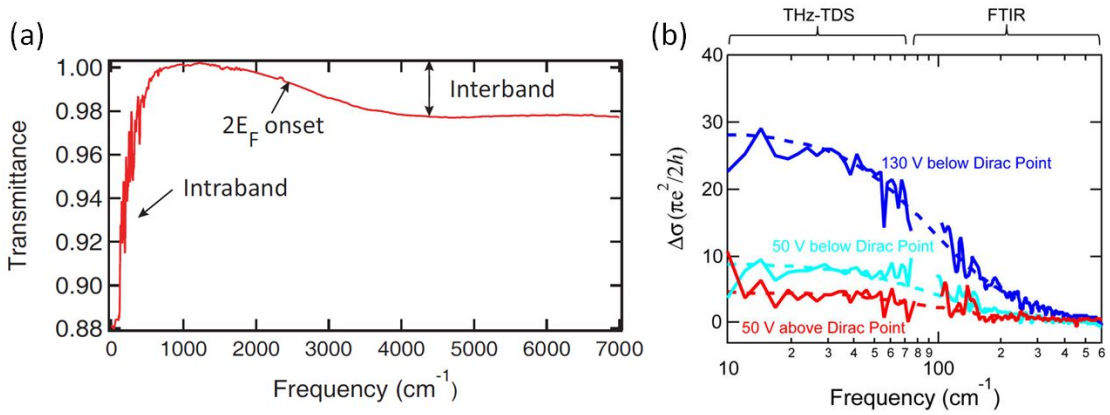

Figure 4. (a) Transmittance spectrum of single-layer graphene showing intraband and interband absorption with the "$2E_F$ onset" for interband absorption. (b) Gate-induced sheet conductance change for intraband dynamics in the THz regime. Adapted from Ref. [8].

Here, we studied the THz and infrared transmission of large-area graphene in a field-effect transistor (FET) configuration, consisting of a single layer graphene (SGL) on a SiO_2/p-Si substrate. A typical transmittance spectrum is shown in Fig. 4a. We observed both the strongly frequency-dependent intraband absorption in the THz range and frequency-independent (universal) interband absorption in the mid-infrared (MIR) range. Furthermore, we measured the dynamic conductivity change in the THz region induced by electrical gating, as shown in Fig. 4b, where the position of the Fermi energy was deduced by theoretical fits.[8] Based on Fig. 4b, one can see that, when a gate voltage is applied, the Fermi level moves away from the Dirac point and the overall conductance increases due to the increase of carrier density. These results demonstrate promising functionalities of large-area graphene devices for critical components in THz and infrared optoelectronics.

5. TERAHERTZ OPTOELERONIC DEVICES BASED ON GRAPHENE

5.1 Graphene Plasmonic Device

Graphene has been shown to support surface plasmon polaritons (SPPs) with strong confinement and low propagation loss in the mid-infrared region due to its large carrier mobilities at room temperature.[36] The carrier density in graphene is highly gate-tunable, which can achieve tuning times below one nanosecond.[37] These properties make graphene a promising material for electrically tunable plasmonic devices. The key challenge associated with efficient excitation of SPPs in graphene is to compensate the momentum difference between the SPPs and the incident electromagnetic beam.[38] One widely-used scheme is grating coupling, where the periodicity of the grating provides the additional in-plane momentum needed to excite the SPP.[39] Here, we demonstrate the excitation and active control of SPPs in graphene using a silicon grating.

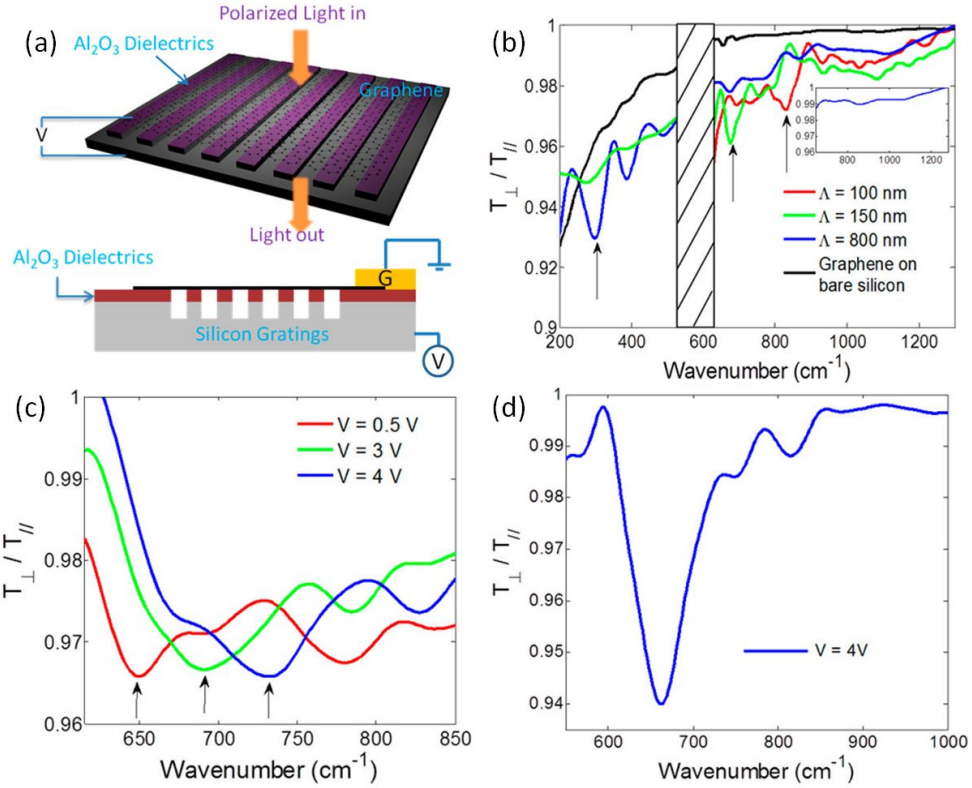

Figure 5. Polarized transmission measurements of gated graphene plasmoinc devices. (a) Schematic of normal-incidence transmission measurement of silicon-grating-assisted graphene plasmon excitation by guided-wave resonance (GWR) with two polarizations ($T_\perp$ and $T_{//}$). (b) Transmission spectra in the THz (200-550 cm^{-1}) and MIR (620-1300 cm^{-1}) for different grating periods. The resonance dips are marked by arrows. The black line is the transmittance of monolayer graphene. The shaded area represents the frequency region where the signal-to-noise ratio was too low. Inset is the transmission spectrum of grating period Λ = 800 nm in the MIR without graphene. (c) Electrical tuning of the fabricated GWR graphene plasmonic device with period Λ = 100 nm. The resonance dips are marked by arrows. (d) The response of a grpahene plasmonic device with period Λ = 100 nm under a bias of 4 V, which reaches an extinction ratio of ~6%. Adapted from Ref. [9].

Shown in Fig. 5a is a sketch of the device architecture. The fabrication procedure included the following steps: i) periodically spaced tranches were etched into a lightly doped silicon substrate for grating formation; the depth and length of each trench were ~ 250 nm and ~ 60 μm, respectively, and the grating period (Λ) varied from device to device; ii) a 30-nm-thick layer of aluminum oxide was then deposited on top of the grating as the dielectric material; and iii) CVD-grown SGL was transferred on top of the grating as the propagating medium of SPPs. The silicon grating served for two purposes: i) facilitating SSP excitation in graphene under the normal-incidence of infrared beam through the guide-wave resonance (GWR)[9, 39] and ii) tuning the resonance frequency of the device over a wide spectral range by acting as back gate electrodes. Polarization-dependent transmission experiments in the mid-infrared (MIR) and far-infrared (FIR) regions were performed on devices with different grating periods, as shown in Fig. 5b. As the SSPs can only be excited when the input light is polarized perpendicular to the grating lines, the dependence of the ratio $T_\perp/T_{//}$ on the frequency show a series of resonant dips, indicating light energy is absorbed in the graphene layer due to the excitation of the SPPs. While the resonance frequency can be changed by the gating period, it can also be modulated through electrical gating at a fixed grating period. As shown in Fig. 5c, a large shift of ~80 cm^{-1} is reached by increasing the gate voltage from 0.5 to 4 V. The ER of the resonance varied from device to device, presumably due to sample uniformity variations. A high ER of ~0.6% was achieved on the device with grating period Λ = 200 nm and bias voltage of 4 V, as shown in Fig. 5d. These results pave the way to excite and actively control plasmonic waves in graphene.

5.2 Graphene Terahertz Modulator

Because its novel two-dimensional nature, the electronic properties of graphene are highly gate-controllable, opening the possibility of diverse device applications.[40-43] One of the promising applications is to build a graphene-based THz modulator.[42] To date, however, its small non-resonant intraband absorption has been the bottleneck of developing graphene THz modulators with high extinction ratios. Recently, many efforts have been put to enhance the SLG absorption in the THz region, such as exciting plasmonic resonance in graphene,[44] integrating graphene with photonic cavities[43] or metamaterials.[45] Here, we show a novel graphene THz modulator with a large modulation depth, a high speed, and a designable resonance frequency.

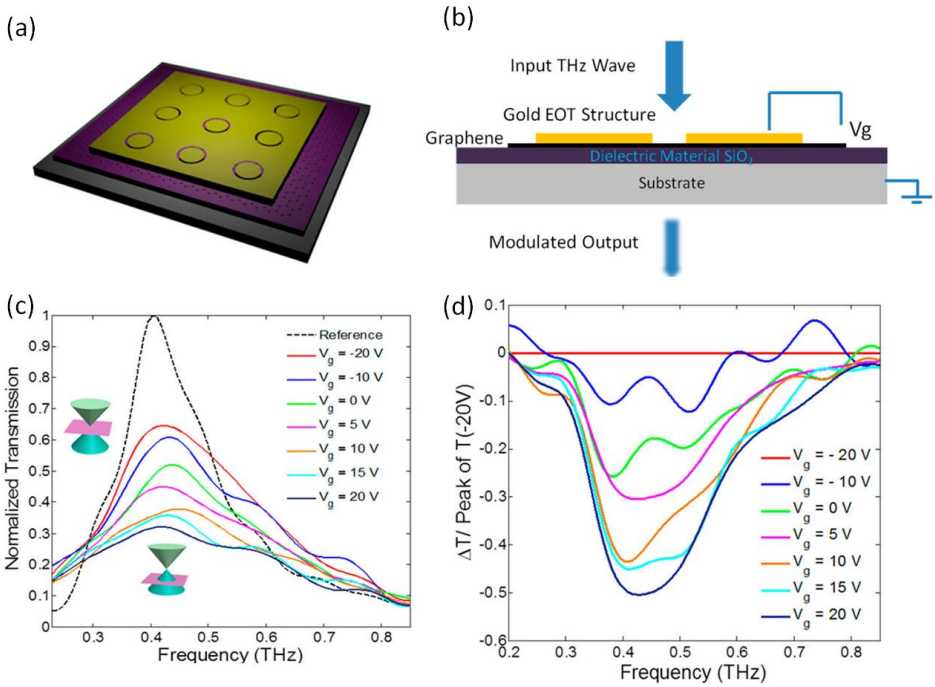

Figure 6. (a) Schematic diagram of the EOT graphene-based THz modulator. (b) Cross section of the modulator. Graphene is placed on a SiO_2/Si substrate, and the EOT structure is fabricated on top of graphene. (c) Transmission spectra for the EOT graphene-based THz modulator under different gate voltages between -20 V and +20 V. (d) The transmission change at different gate voltages. A large modulation depth of ~50% is obtained. Adapted from Ref. [10].

Taking advantage of the extraordinary optical transmission (EOT) effect,[46] we used a metallic film with sub-wavelength apertures to enhance the extinction ratio of the graphene-based THz modulator. To fabricate the device, we first transferred the CVD-grown SLG onto a SiO_2/Si substrate using a poly(methylmethacrylate) (PMMA)-assisted wet-transfer technique. Metallic films (3-nm-thick titanium and 97-nm thick gold) were successively evaporated onto the surface of SLG using e-beam evaporation, in which the EOT array with ring shaped structures were defined by e-beam lithography (see Figs. 6a and 6b). A series of THz transmission spectra were measured on the device with different bias gate voltages, in the range from −20 V to 20 V, as shown in Fig. 6c. One can find that the aperture-induced resonance is centered at ~0.44 THz, and the value of peak transmission changes with the gate voltage. According to Fig. 6d, a large modulation depth of ~50% is achieved, where ΔT was defined as $T(V_g) - T(-20\text{V})$ and normalized to the peak of T (−20V). In addition, the estimated speed of the device is as large as ~0.2 GHz by taking into account the device capacitance. Moreover, by changing the circumference of the apertures, the EOT array could be scaled to have different resonance frequencies over a wide THz range. These results suggest the possibility of CMOS-compatible THz modulators based on graphene with a large ER, a high speed, and a tailored working frequency.

ACKNOWLEDGEMENT

This work was supported by the Department of Energy (through Grant No. DE-FG02-06ER46308), the National Science Foundation (through Grants No. OISE-0968405), and the Robert A. Welch Foundation (through Grant No. C-1509). Some of the work presented in this article was performed in collaboration with P. M. Ajayan, A. A. Belyanin, E. H. Hároz, R. H. Hauge, D. M. Mittleman, M. Tonouchi, J. M. Tour, R. Vajtai, and Q. Xu.

REFERENCES

[1] M. Lee, and M. C. Wanke, "Searching for a solid-state terahertz technology," Science, 316(5821), 64-65 (2007).

[2] P. Avouris, M. Freitag, and V. Perebeinos, "Carbon-nanotube photonics and optoelectronics," Nature Photonics, 2(6), 341-350 (2008).

[3] F. Bonaccorso, Z. Sun, T. Hasan *et al.*, "Graphene photonics and optoelectronics," Nature Photonics, 4(9), 611-622 (2010).

[4] R. R. Hartmann, J. Kono, and M. Portnoi, "Terahertz science and technology of carbon nanomaterials," Nanotechnology, 25(32), 322001 (2014).

[5] Q. Zhang, E. H. Hároz, Z. Jin *et al.*, "Plasmonic nature of the terahertz conductivity peak in single-wall carbon nanotubes," Nano Letters, 13(12), 5991-5996 (2013).

[6] L. Ren, C. L. Pint, T. Arikawa *et al.*, "Broadband terahertz polarizers with ideal performance based on aligned carbon nanotube stacks," Nano Letters, 12(2), 787-790 (2012).

[7] X. He, N. Fujimura, J. M. Lloyd *et al.*, "Carbon nanotube terahertz detector," Nano Letters, 14(7), 3953-3958 (2014).

[8] L. Ren, Q. Zhang, J. Yao *et al.*, "Terahertz and infrared spectroscopy of gated large-area graphene," Nano Letters, 12(7), 3711-3715 (2012).

[9] W. Gao, G. Shi, Z. Jin *et al.*, "Excitation and active control of propagating surface plasmon polaritons in graphene," Nano Letters, 13(8), 3698-3702 (2013).

[10] W. Gao, J. Shu, K. Reichel *et al.*, "High-contrast terahertz wave modulation by gated graphene enhanced by extraordinary transmission through ring apertures," Nano Letters, 14(3), 1242-1248 (2014).

[11] M. Bockrath, D. H. Cobden, J. Lu *et al.*, "Luttinger-liquid behaviour in carbon nanotubes," Nature, 397(6720), 598-601 (1999).

[12] A. Ugawa, A. G. Rinzler, and D. Tanner, "Far-infrared gaps in single-wall carbon nanotubes," Physical Review B, 60(16), R11305 (1999).

[13] M. Itkis, S. Niyogi, M. Meng *et al.*, "Spectroscopic study of the Fermi level electronic structure of single-walled carbon nanotubes," Nano Letters, 2(2), 155-159 (2002).

[14] T. Kampfrath, K. von Volkmann, C. Aguirre *et al.*, "Mechanism of the far-infrared absorption of carbon-nanotube films," Physical Review Letters, 101(26), 267403 (2008).

[15] N. Akima, Y. Iwasa, S. Brown *et al.*, "Strong Anisotropy in the Far‐Infrared Absorption Spectra of Stretch‐Aligned Single‐Walled Carbon Nanotubes," Advanced Materials, 18(9), 1166-1169 (2006).

[16] L. Ren, Q. Zhang, C. Pint *et al.*, "Collective antenna effects in the terahertz and infrared response of highly aligned carbon nanotube arrays," Physical Review B, 87, 161401 (2013).

[17] G. Y. Slepyan, M. Shuba, S. Maksimenko *et al.*, "Terahertz conductivity peak in composite materials containing carbon nanotubes: Theory and interpretation of experiment," Physical Review B, 81(20), 205423 (2010).

[18] L. Ren, C. L. Pint, L. G. Booshehri *et al.*, "Carbon nanotube terahertz polarizer," Nano Letters, 9(7), 2610-2613 (2009).

[19] L. Yang, S. Wang, Q. Zeng *et al.*, "Carbon nanotube photoelectronic and photovoltaic devices and their applications in infrared detection," Small, 9(8), 1225-1236 (2013).

[20] M. E. Itkis, F. Borondics, A. Yu *et al.*, "Bolometric infrared photoresponse of suspended single-walled carbon nanotube films," Science, 312(5772), 413-416 (2006).

[21] A. Y. Glamazda, V. Karachevtsev, W. B. Euler *et al.*, "Achieving High Mid‐IR Bolometric Responsivity for Anisotropic Composite Materials from Carbon Nanotubes and Polymers," Advanced Functional Materials, 22(10), 2177-2186 (2012).

[22] X. He, X. Wang, S. Nanot *et al.*, "Photothermoelectric p–n Junction Photodetector with Intrinsic Broadband Polarimetry Based on Macroscopic Carbon Nanotube Films," ACS Nano, 7(8), 7271-7277 (2013).
[23] B. C. St-Antoine, D. Ménard, and R. Martel, "Single-walled carbon nanotube thermopile for broadband light detection," Nano Letters, 11(2), 609-613 (2010).
[24] Y. Nakai, K. Honda, K. Yanagi *et al.*, "Giant Seebeck coefficient in semiconducting single-wall carbon nanotube film," Applied Physics Express, 7(2), 025103 (2014).
[25] C. Hu, C. Liu, L. Chen *et al.*, "A demo opto-electronic power source based on single-walled carbon nanotube sheets," ACS Nano, 4(8), 4701-4706 (2010).
[26] Y. Nonoguchi, K. Ohashi, R. Kanazawa *et al.*, "Systematic conversion of single walled carbon nanotubes into n-type thermoelectric materials by molecular dopants," Scientific Reports, 3, (2013).
[27] G. Fedorov, A. Kardakova, I. Gayduchenko *et al.*, "Photothermoelectric response in asymmetric carbon nanotube devices exposed to sub-terahertz radiation," Applied Physics Letters, 103(18), 181121 (2013).
[28] K. Fu, R. Zannoni, C. Chan *et al.*, "Terahertz detection in single wall carbon nanotubes," Applied Physics Letters, 92(3), 033105 (2008).
[29] M. Rinzan, G. Jenkins, H. Drew *et al.*, "Carbon nanotube quantum dots as highly sensitive terahertz-cooled spectrometers," Nano Letters, 12(6), 3097-3100 (2012).
[30] H. Hortensius, A. Öztürk, P. Zeng *et al.*, "Microwave-induced nonequilibrium temperature in a suspended carbon nanotube," Applied Physics Letters, 100(22), 223112 (2012).
[31] K. F. Mak, M. Y. Sfeir, Y. Wu *et al.*, "Measurement of the optical conductivity of graphene," Physical Review Letters, 101(19), 196405 (2008).
[32] R. Nair, P. Blake, A. Grigorenko *et al.*, "Fine structure constant defines visual transparency of graphene," Science, 320(5881), 1308-1308 (2008).
[33] Z. Li, E. A. Henriksen, Z. Jiang *et al.*, "Dirac charge dynamics in graphene by infrared spectroscopy," Nature Physics, 4(7), 532-535 (2008).
[34] H. Yan, F. Xia, W. Zhu *et al.*, "Infrared spectroscopy of wafer-scale graphene," ACS Nano, 5(12), 9854-9860 (2011).
[35] W. Liu, R. V. Aguilar, Y. Hao *et al.*, "Broadband microwave and time-domain terahertz spectroscopy of chemical vapor deposition grown graphene," Journal of Applied Physics, 110(8), 083510 (2011).
[36] I. Maeng, S. Lim, S. J. Chae *et al.*, "Gate-controlled nonlinear conductivity of Dirac fermion in graphene field-effect transistors measured by terahertz time-domain spectroscopy," Nano Letters, 12(2), 551-555 (2012).
[37] M. Liu, X. Yin, E. Ulin-Avila *et al.*, "A graphene-based broadband optical modulator," Nature, 474(7349), 64-67 (2011).
[38] Z. Fei, A. Rodin, G. Andreev *et al.*, "Gate-tuning of graphene plasmons revealed by infrared nano-imaging," Nature, 487(7405), 82-85 (2012).
[39] W. Gao, J. Shu, C. Qiu *et al.*, "Excitation of plasmonic waves in graphene by guided-mode resonances," ACS Nano, 6(9), 7806-7813 (2012).
[40] F. Xia, T. Mueller, Y.-m. Lin *et al.*, "Ultrafast graphene photodetector," Nature Nanotechnology, 4(12), 839-843 (2009).
[41] L. Vicarelli, M. Vitiello, D. Coquillat *et al.*, "Graphene field-effect transistors as room-temperature terahertz detectors," Nature Materials, 11(10), 865-871 (2012).
[42] B. Sensale-Rodriguez, R. Yan, M. M. Kelly *et al.*, "Broadband graphene terahertz modulators enabled by intraband transitions," Nature Communications, 3, 780 (2012).
[43] B. Sensale-Rodriguez, R. Yan, S. Rafique *et al.*, "Extraordinary control of terahertz beam reflectance in graphene electro-absorption modulators," Nano Letters, 12(9), 4518-4522 (2012).
[44] L. Ju, B. Geng, J. Horng *et al.*, "Graphene plasmonics for tunable terahertz metamaterials," Nature Nanotechnology, 6(10), 630-634 (2011).
[45] S. H. Lee, M. Choi, T.-T. Kim *et al.*, "Switching terahertz waves with gate-controlled active graphene metamaterials," Nature Materials, 11(11), 936-941 (2012).
[46] M. Seo, H. Park, S. Koo *et al.*, "Terahertz field enhancement by a metallic nano slit operating beyond the skin-depth limit," Nature Photonics, 3(3), 152-156 (2009).